Dynamics of supported ultrathin molybdenum films driven by strong short laser impact

V A Khokhlov[1], Yu V Petrov[1,2], N A Inogamov[1,3], K P Migdal[3,1], J Winter[4,5,6], C Aichele[4], S Rapp[4,5,6] and H P Huber[4]

[1] Landau Institute for Theoretical Physics of the Russian Academy of Sciences, Akademika Semenova 1a, Chernogolovka, Moscow Region 142432, Russia
[2] Moscow Institute of Physics and Technology, Institutskiy Pereulok 9, Dolgoprudny, Moscow Region 141700, Russia
[3] Dukhov Research Institute of Automatics (VNIIA), Sushchevskaya 22, Moscow 127055, Russia
[4] Department of Applied Sciences and Mechatronics, Munich University of Applied Sciences, Lothstraße 34, Munich 80335, Germany
[5] Erlangen Graduate School in Advanced Optical Technologies, Friedrich-Alexander-Universität Erlangen-Nürnberg, Paul-Gordan-Straße 6, Erlangen 91052, Germany
[6] Lehrstuhl für Photonische Technologien, Friedrich-Alexander-Universität Erlangen-Nürnberg, Konrad-Zuse-Straße 3-5, Erlangen 91052, Germany

E-mail: nailinogamov@gmail.com

Abstract. We consider expansion, break off, and flight of 10 nm molybdenum film deposited onto glass support. These events are initiated by action of subpicosecond laser pulse onto film. Approximations for two-temperature equation of state and electron–ion coupling parameter are developed. Heat conduction is unimportant because film is ultrathin and because radius of a laser beam is rather large $\sim$ 10 μm (thus lateral thermal spreading is insignificant at the considered time scale). We use two-temperature one-dimensional hydrodynamic code to follow evolution of laser induced flow. Additional code for treating transmission and reflection of a monochromatic electromagnetic wave is developed. It is applied to describe interference between transmitted and reflected waves in the layered structure appearing thanks to laser induced expansion and separation of a film.

1. Introduction

Important direction in physics of laser–matter interaction is connected with ultrashort laser pulses (UsLP). There are three ranges of their fluences F: weak, moderate, and strong. The range of moderate fluences begins around melting threshold $F_{\rm m}$ for bulk metal targets and continues up to $\sim (10^2$–$10^3)F_{\rm m}$, see [1]. In absorbed fluences $F_{\rm abs}$, the melting threshold $F_{\rm abs}|_{\rm m}$ is of the order of few tens of mJ/cm^2 for bulk metal targets. There are two subranges of high fluences above the moderate range. They are below [2,3] and above [4–6] the relativistic intensity $\sim 10^{18}$–10^{19} W/cm^2. At this intensity the quivering kinetic energy of electron oscillations in a laser electromagnetic wave $\lambda_1^2 I_{18}\times 90$ keV becomes of the order of the rest energy of electron while amplitude of electron oscillations in vacuum $\lambda_1^2\sqrt{I_{18}}\times 100$ nm becomes larger than thickness

$d_{\rm skin} = 10$–20 nm of a skin-layer, here $\lambda_1 = \lambda/1\ \mu$m is wavelength of a wave, $I_{18} = I/10^{18}$ W/cm^2 is its intensity.

Below we consider the moderate range of the laser actions. With UsLP new physics of laser ablation appears. This is the thermomechanical ablation. It differs qualitatively from previously known ablation by subnanosecond and nanosecond pulses which are of the purely evaporative origin. The first manifestation (1998, 1999) about the principal change of the origin comes from observation of Newton rings rising their number with time [7–9]. Thermomechanical ablation was also observed in molecular dynamics (MD) simulations of laser heating of soft tissues [10].

Duration $\tau_{\rm L}$ of UsLP is less than ~ 1 ps. In this case we have to include into consideration a finite time relaxation between electron and ion subsystems of a metal [11]. During UsLP the laser energy is absorbed by electrons. Thus the electron subsystem becomes hotter than the ion one: $T_{\rm e} > T_{\rm i}$, where $T_{\rm e}$ and $T_{\rm i}$ are electron and ion temperatures. This is the two-temperature (2T) case important for UsLP. Thanks to electron–ion coupling the temperatures $T_{\rm e}$ and $T_{\rm i}$ equalize gradually [11, 12] during equilibration time $t_{\rm eq}$. It should be mentioned that duration of equilibration $t_{\rm eq}$ depends on thickness of a target $d_{\rm f}$ relative to thickness $d_{\rm T}$ ($d_{\rm T} > d_{\rm skin}$) of a heat affected zone in a bulk target. For thick targets $d_{\rm f} > d_{\rm T}$ the electron temperature $T_{\rm e}$ in large extent drops down thanks to electron heat conduction from a skin $d_{\rm skin}$ to a heat affected zone $d_{\rm T}$; $d_{\rm T} > d_{\rm skin}$. While for thin films $d_{\rm f} \ll d_{\rm T}$ the conductive loses are insignificant, and duration $t_{\rm eq}$ is longer, because only electron–ion coupling contributes to decrease of $T_{\rm e}$ and to drawing together the temperatures $T_{\rm e}$ and $T_{\rm i}$.

The first paper introduced the 2T states $T_{\rm e} > T_{\rm i}$ in laser irradiated condensed matter was [11]. Significantly later on the laser systems based on chirped pulse amplification and generating UsLPs appear [13] and the approach with 2T states becomes popular [1–3, 12, 14–20] because people began to use action of UsLP onto targets while the 2T approach allows them to describe results of laser–matter interaction. Experiments in the nineties operated with rather weak UsLPs, thus electrons were overheated above lattice to a few thousand Kelvins and electron energy per unit of volume and pressure were rather small. Later on more strong actions became possible, they cause overheating to a few tens of kiloKelvins and may cause the thermomechanical ablation.

Inclusion of electronic contribution to thermodynamics of condensed matter was proposed in the fifties–sixties [21–26]:

$$f = f_{\rm i} + f_{\rm e}, \tag{1}$$

where f, $f_{\rm i}$, and $f_{\rm e}$ are free energies of whole system and its ionic and elecronic contributions. This allows to develope the one-temperature (1T),

$$T_{\rm e} = T_{\rm i} = T, \tag{2}$$

wide-range equations of states (EoS) for *high* temperatures where the electronic contribution becomes significant thanks to excitation of electrons [27, 28]. Let us mention that the paper [11] breaks the condition (2) and separates independent temperatures. For low temperatures T in (2) the electronic excitations are weak and the electronic addition $f_{\rm e}$ in (1) to EoS is insignificant. What temperatures are low in the sense that $f \approx f_{\rm i} \ll f_{\rm e}$?

Critical temperatures $T_{\rm c}$ of metals, especially rarefactory metals, are rather high. Let us show that at the temperatures $\approx T_{\rm c}$ the contribution $f_{\rm e}$ is important. Estimates based on Fermi theory of free electrons show that

$$P_{\rm e} = \gamma T_{\rm e}^2/3, \qquad c_{\rm e} = \gamma T_{\rm e}, \qquad \gamma = \gamma_0 (n_{\rm e}/n_{\rm e0})^{1/3}, \tag{3}$$

here $c_{\rm e}$ is a heat capacity of an electron subsystem per unit volume, $n_{\rm e} = Zn$ is electron concentration, n is atomic concentration, $n_{\rm e0}$ is electron concentration at solid state density. We have

$$n_{\rm c} \approx (1/3\text{–}1/4) n_0, \qquad T_{\rm c} \approx 10^4 \text{ K}, \qquad \gamma_0 \sim 100 \text{ J/m}^3/\text{K}^2. \tag{4}$$

Using (3) and (4), supposing that the charge Z remains fixed during this range of expansions, and taking $Z = 1$, we obtain the electron pressure at critical parameters $P_{\rm e}|_{\rm c} \approx 2$ GPa.

While critical temperature of Mo is 11.8 kK according to [29]. It is slightly higher than the isotherm 10^4 K. Quantum molecular dynamics (QMD) simulations [29] give unusually large degree of expansion ≈ 6.5 between critical and normal density points. Approximation (1) together with Mie–Grüneisen approach implies that EoS may be split up into three contributions

$$f(\rho, T_{\rm e}, T_{\rm i}) = f_{\rm s}(\rho) + \phi_{\rm i}(\rho, T_{\rm i}) + \phi_{\rm e}(\rho, T_{\rm e}). \tag{5}$$

Thus separation of temperatures $T_{\rm i}$ and $T_{\rm e}$ essentially splits the Mie–Grüneisen thermal contribution ϕ into electron and ion parts together with the cold (static) contribution (we neglect zero-point vibrational functions in comparison with the static functions and thermal exitations). The contributions $\phi_{\rm i}(\rho, T_{\rm i})$ and $\phi_{\rm e}(\rho, T_{\rm e})$ may be approximately factorized into density and temperature dependent factors. Thus electron and ion Grüneisen parameters $\Gamma_{\rm e}$ and $\Gamma_{\rm i}$ appear.

Electron addition to pressure $P_{\rm e}$ has a thermal nature. It much weaklier depends on density relative to cold pressure. Therefore pressure $P_{\rm e}$ remains significant at rather large (few times) volume extensions, see (3), (4). Estimates (3), (4) give $P_{\rm e}|_{\rm crit} \approx 2$ GPa. This estimate are few times larger than critical pressure $P_{\rm c} \approx 0.7$ GPa [29]. Negative ion pressures $P_{\rm i}(\rho, T_{\rm i}) < 0$ are necessary to decrease total pressure to $P_{\rm c}$.

Values $P_{\rm i}(\rho, T_{\rm i}) < 0$ are usual for metastable stretched states [30] and for physics of UsLP with 2T states. Let us compare two phase coexistence boundaries (binodal, bin) for 1T (2) and 2T states:

$$\rho_{\rm bin-1T}, T_{\rm e} = T_{\rm bin-1T}, T_{\rm i} = T_{\rm bin-1T}; \qquad \rho_{\rm bin-2T}, T_{\rm e\,bin-2T}, T_{\rm i\,bin-2T} = T_{\rm bin-1T}; \qquad T_{\rm e\,bin-2T} > T_{\rm bin-1T}. \tag{6}$$

Additional excitation of electrons rises their positive pressure which additionally expands ion subsystem in equilibrium conditions where total pressure is small. Therefore the 2T coexistence boundary (6) is shifted to smaller densities

$$\rho_{\rm bin-2T} < \rho_{\rm bin-1T}$$

relative to the 1T coexistence boundary at the same ion temperature $T_{\rm i} = T_{\rm bin-1T}$ and elevated electron temperatures $T_{\rm e\,bin-2T} > T_{\rm bin-1T}$ [31–35], see also figures 18–22 in [36]. Equilibrium 2T states which can contact with saturated vapor disappear for electron temperatures higher than 20–25 kK at the any (even low $T_{\rm i} = 0$) ion temperatures for all studied metals from Ni and Ta to Au and Cu [31–34,36]. This corresponds to the near critical region of 2T EoS. Metal transfers to the supercritical 2T fluid state above (that is at higher temperatures) this region. Difference between liquid and vapor eliminates in the supercritical 2T states. It is supposed that atoms transit from condensed to vapor states keeping their degree of electron excitation during 2T evaporation. Problem of 2T saturated vapor needs special discussion.

In this paper Mie–Grüneisen two-temperature approach is applied to describe two-temperature thermodynamical characteristics of molybdenum in the process of its ablation under the action of femtosecond laser pulses. Molybdenum is the essential constructive element of the pump–probe laser optical schemes. It refers to metals with a high melting point. In this work we consider a thin molybdenum film (10 nm thickness) deposited on a glass substrate (of 500 μm thickness). This design is a target for the femtosecond laser impulse within the pump–probe scheme. Infrared probe pulse has a light wave length 1053 nm while the wave length of the probe pulse is 527 nm. We are interesting in a interference pattern produced by the probe pulse during the process of ablation after the action of the pump pulse. If we consider this interference in the small vicinity of the center of laser spot on the target, the ablation pattern with the sufficient accuracy can be represented as one-dimensional. This one-dimensional ablative motion of a target matter we investigate with the use of a hydrodynamical

code. This code calculates parameters of the moving matter by the use of its two-temperature thermodynamics and two-temperature kinetics. State of the ablative matter, distribution of its velocity, density, temperature defines the interference picture produced by the probe pulse. We calculate the temporal evolution of this interference picture on the multilayer ablative formation.

2. Thermodynamic functions of molybdenum

We shall consider thermodynamic functions of molybdenum in the framework of Mie–Grüneisen approach. In the two-temperature state with the temperatures of ions T_i and the temperature of electrons T_e internal energy will be presented as a sum

$$E(x, T_\mathrm{i}, T_\mathrm{e}) = E_\mathrm{i}(x, T_\mathrm{i}) + E_\mathrm{e}(x, T_\mathrm{e}),$$

where its ionic part

$$E_\mathrm{i}(x, T_\mathrm{i}) = E_\mathrm{s}(x) + E_\mathrm{T}(x, T_\mathrm{i})$$

consists of the static energy $E_\mathrm{s}(x)$ and the thermal part $E_\mathrm{T}(x, T_\mathrm{i})$. Here we have inroduced the relative density of the material $x = \rho/\rho_0$, where ρ_0 is the density at zero temperature and pressure. According to our calculations based on the density functional theory (DFT), it corresponds to the volume per atom $v_0 = 105.47 a_\mathrm{B}^3$ (a_B is the Bohr radius). Electronic part $E_\mathrm{e}(x, T_\mathrm{e})$ describes the contribution of the excited electrons into the internal energy.

The static energy is chosen in the form consisting of the repulsive part at the small values of x and interaction at large x and as a quantity per atom is

$$E_\mathrm{s}(x) = A\left(\frac{x^a}{a} - \frac{x^b}{b}\right)$$

with $a > b$. And the thermal part of the ionic energy (per atom) is simply

$$E_\mathrm{T}(x, T_\mathrm{i}) = 3k_\mathrm{B}T_\mathrm{i}$$

with k_B being the Boltzmann constant and both the ion as the electron temperature to be measured in K.

Another thermodynamic function important at the hydrodynamics research of the laser ablation of materials is the pressure which within the same approach is

$$P(x, T_\mathrm{i}, T_\mathrm{e}) = P_\mathrm{i}(x, T_\mathrm{i}) + P_\mathrm{e}(x, T_\mathrm{e})$$

with the ionic part

$$P_\mathrm{i}(x, T_\mathrm{i}) = P_\mathrm{s}(x) + P_\mathrm{T}(x, T_\mathrm{i}).$$

Here

$$P_\mathrm{s}(x) = \frac{A}{v_0} x(x^a - x^b) \tag{7}$$

is the static pressure, and

$$P_\mathrm{T}(x, T_\mathrm{i}) = \frac{3k_\mathrm{B}T_\mathrm{i}}{v_0} xG(x)$$

is the thermal part of pressure. Grüneisen parameter $G(x)$ of the solid phase of metal is $G(x) = \mathrm{d}\ln\theta/\mathrm{d}\ln x$ with $\theta(x)$ being the Debye temperature. The Debye temperature $\theta = \hbar s(x) k_\mathrm{D}(x)/k_\mathrm{B}$, where $s(x)$ and $k_\mathrm{D}(x)$ are the sound speed and Debye wave number. Taking into account that $k_\mathrm{D} \propto x^{1/3}$ and

$$s(x) \propto \sqrt{\frac{\partial P_\mathrm{s}}{\partial \rho}} \propto \sqrt{\frac{\partial P_\mathrm{s}}{\partial x}} \propto \sqrt{(a+1)x^a - (b+1)x^b},$$

we obtain

$$G(x) = \mathrm{d}\ln\theta/\mathrm{d}\ln x = \frac{1}{3} + \frac{1}{2}\frac{a(a+1)x^a - b(b+1)x^b}{(a+1)x^a - (b+1)x^b}. \tag{8}$$

To avoid divergence of this expression at small x we change it to a close expression [37]

$$G(x) = \frac{5}{6} + \frac{2a(b+1) + (a-b)(a-1)x^{a+1}}{2(b+1+(a-b)x^{a+1})}. \tag{9}$$

Functions (8) and (9) have equal values and equal values of their derivatives at $x = 1$.

The electron contribution to the internal energy and pressure $E_\mathrm{e}(x, T_\mathrm{e})$ and $P_\mathrm{e}(x, T_\mathrm{e})$ was calculated in the VASP program of the density functional method as the difference between the values of energy and pressure at electron temperature T_e and at a low electron temperature. The results of these calculations for the electron internal energy per unit volume can be approximated in the form of expression

$$E_\mathrm{e}(x, T_\mathrm{e}) = e_{\mathrm{e}1} x^{5/3}(\sqrt{\tau^2 + \tau_e^2} - \tau_e).$$

Here we have introduced dimensionless variable $\tau = T_\mathrm{e}/(T_{a6}x^{2/3})$ (electron temperature T_e is measured in K), $T_{a6} = 6T_{a1}$, $T_{a1} = 11605$ K, $e_{\mathrm{e}1} = 244.9$ GPa, $\tau_e = 0.1508$. Accordingly elecronic part of pressure can be approximated as

$$P_\mathrm{e}(x, T_\mathrm{e}) = p_{\mathrm{e}1} x^{5/3}(\sqrt{\tau^2 + \tau_p^2} - \tau_p)$$

with $p_{\mathrm{e}1} = 235.1$ GPa, $\tau_p = 0.08507$.

From the expression (7) for the static pressure the minimal static pressure $-p_m$ can be found. Minimumal value of the pressure (7) takes place at the compression

$$x_m = \Big(\frac{b+1}{a+1}\Big)^{\frac{1}{a-b}}$$

and is equal to

$$-p_m = \frac{A}{v_0}(b-a)\left[\frac{(b+1)^{b+1}}{(a+1)^{a+1}}\right]^{\frac{1}{a-b}}.$$

Then the parameter A can be expressed through the p_m value:

$$A = \frac{p_m v_0}{a-b}\left[\frac{(a+1)^{a+1}}{(b+1)^{b+1}}\right]^{\frac{1}{a-b}}. \tag{10}$$

Our DFT calculations consistent with other data [38, 39] give $p_m = 40$ GPa. With the help of (10) there are only two free parameters—a and b for the ionic part of energy and pressure. They were calculated to reproduce the zero pressure isobar obtained by the use of quantum molecular dynamics in [29]. Considering the zero pressure isobar, we have $P = P_\mathrm{i} + P_\mathrm{e} = 0$. Substituting here expressions for the ionic and electronic parts of pressure, in the equilibrium state with the temperature $T = T_\mathrm{i} = T_\mathrm{e}$ we obtain

$$\frac{A}{v_0}x(x^a - x^b) + \frac{3k_\mathrm{B}T}{v_0}xG(x) + p_1 x^{5/3}\Big(\sqrt{\Big(\frac{k_\mathrm{B}T}{T_{a6}x^{2/3}}\Big)^2 + \tau_p^2} - \tau_p\Big) = 0. \tag{11}$$

By introducing the notations

$$w_1 = \frac{A}{v_0}x(x^a - x^b),$$
$$w_2 = \frac{3}{v_0},$$
$$w_3 = p_1 x^{5/3},$$
$$w_4 = \Big(\frac{1}{T_{a6}x^{2/3}}\Big)^2,$$

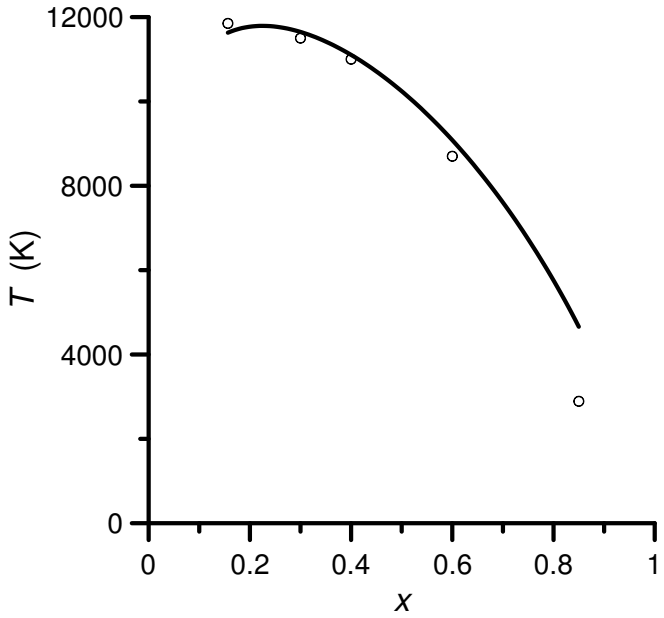

Figure 1. Zero isobar of molybdenum obtained by the use of the equation (12) (solid line) in comparison with the zero isobar from the work [29] (circles).

we obtain from the equation (11) for the dependence of the temperature T on the compression x for the zero pressure isobar

$$k_{\rm B}T = \frac{w_2(w_3b_1 - w_1) - [w_2^2(w_3b_1 - w_1)^2 + w_1(w_2^2 - w_3^2w_4)(2w_3b_1 - w_1)]^{1/2}}{w_2^2 - w_3^2w_4}. \quad (12)$$

From the comparison with the zero pressure isobar obtained in [29] we find values a and b:

$$a = 1.376, \qquad b = 0.176.$$

Then $A = 0.556$ eV from (10). Zero pressure isobar as the dependence of the temperature T on the compression x is presented in figure 1. In figure 2 the Grüneisen parameter (9) with the parameters a and b found is shown together with that one calculated in [40]. In figure 3 several isotherms close to the critical isotherm are drawn. Critical parameters corresponds to

$$x_{\rm c} = 0.126 \ (\rho_{\rm c} = 1.3 \ {\rm g/cm^3}), \qquad T_{\rm c} = 12550 \ {\rm K}, \qquad P_{\rm c} = 1.3 \ {\rm GPa}.$$

In figure 4, some isotherms near the zero-K isotherm are presented. Internal energy and pressure presented were used in the hydrodynamic code to investigate the ablation motion of a thin (10 nm thickness) molybdenum film on the glass substrate (glass thickness is 500 μm).

3. Interference phenomena in the ablation of molybdenum film on the glass

When the thin molybdenum film placed on the glass undergoes an ultrashort laser pulse, it breaks down at sufficient irradiation fluence. Detached part of the film moves away from that remaining on the substrate with the velocity $u_{\rm f}$ while heated and pressurized film on a glass generates the shock wave propagating into the glass with the velocity $u_{\rm s}$. In addition the remainder of the film, initially lying on the glass, begins to separate away from the substrate. This multilayer distribution of a matter creates the interference pattern in the form of Newton rings when the probe laser pulse is exposed to both the metal film side as well as to the glass side. We consider the interference phenomena in the framework of Fresnel theory. Acording to the experimental conditions we consider only the light incidence in the direction, normal to the metal surface. So

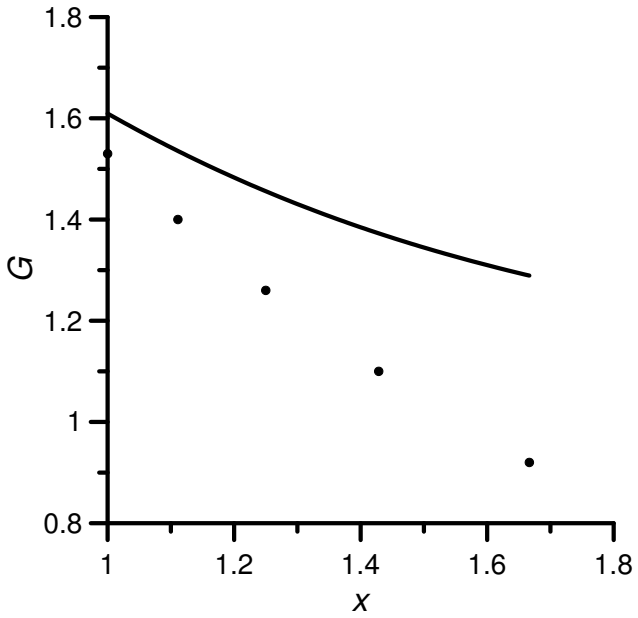

Figure 2. Grüneisen parameter of molybdenum (9) in dependence on the compression x. Circles are the results obtained in [40].

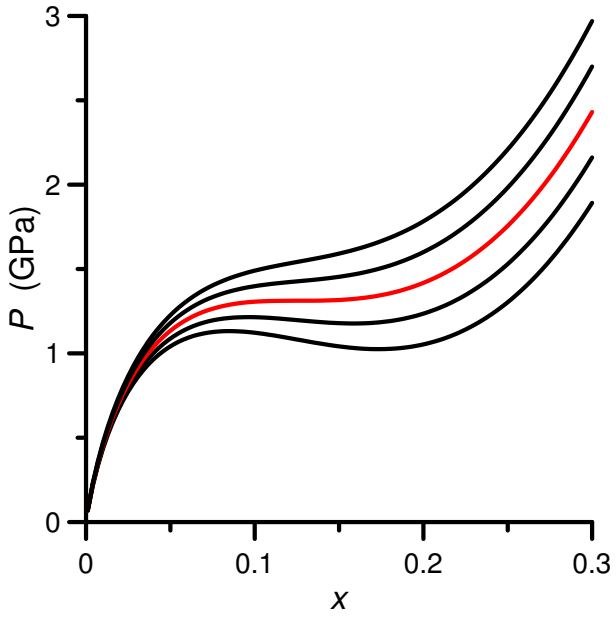

Figure 3. Isotherms of molybdenum close to its critical isotherm (red line). Temperatures at isotherms down up are $T = 12350$, 12450, 12550, 12650 and 12750 K.

the difference between S- and P-polarization of light disappears. For definiteness we consider P-polarization, when the magnetic field vector is perpendicular to the plane of the light of incidence. Vacuum wave length is equal to $\lambda = 527$ nm. Boundary conditions for the electric and magnetic field strength then connect the magnetic field strength in two optical media. We designate in j-layer $H_{\rm t}(j)$ the magnetic field in the wave propagating in the direction of the incident wave and $H_{\rm r}(j)$ in the reflected wave, propagating in the opposite direction. When

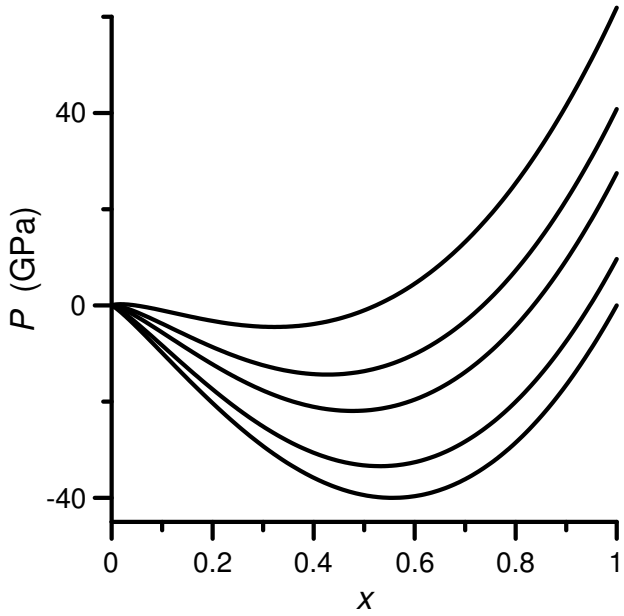

Figure 4. Isotherms of molybdenum at low temperatures. Temperatures down up are 0, 2000, 5000, 7000 and 10000 K.

optical media j and $j+1$ border with each other, then the magnetic field in the medium $j+1$ is expressed through the magnetic field in the medium j as

$$H_{\rm t}(j+1) = b_{\rm tt}(j-1,j)H_{\rm t}(j) + b_{\rm tr}(j-1,j)H_{\rm r}(j), \tag{13}$$

$$H_{\rm r}(j+1) = b_{\rm rt}(j-1,j)H_{\rm t}(j) + b_{\rm rr}(j-1,j)H_{\rm r}(j), \tag{14}$$

where

$$b_{\rm tt}(j-1,j) = \frac{1}{2}\Big(1+\frac{\varepsilon_j}{\varepsilon_{j+1}}\frac{k_j}{k_{j+1}}\Big)\exp[{\rm i}(k_{j+1}-k_j)L_{j,j+1}], \tag{15}$$

$$b_{\rm tr}(j-1,j) = \frac{1}{2}\Big(1-\frac{\varepsilon_j}{\varepsilon_{j+1}}\frac{k_j}{k_{j+1}}\Big)\exp[-{\rm i}(k_{j+1}+k_j)L_{j,j+1}], \tag{16}$$

$$b_{\rm rt}(j-1,j) = \frac{1}{2}\Big(1-\frac{\varepsilon_j}{\varepsilon_{j+1}}\frac{k_j}{k_{j+1}}\Big)\exp[{\rm i}(k_{j+1}+k_j)L_{j,j+1}], \tag{17}$$

$$b_{\rm rr}(j-1,j) = \frac{1}{2}\Big(1+\frac{\varepsilon_j}{\varepsilon_{j+1}}\frac{k_j}{k_{j+1}}\Big)\exp[-{\rm i}(k_{j+1}-k_j)L_{j,j+1}]. \tag{18}$$

In expressions (15)–(18) $\varepsilon_j = \varepsilon_1(j) + {\rm i}\varepsilon_2(j)$ is a complex dielectric permittivity of the medium j, and $k_j = k_{1j} + {\rm i}k_{2j}$ is a complex wave number.

$$k_{1j} = k_0\sqrt{\frac{\sqrt{\varepsilon_1^2(j)+\varepsilon_2^2(j)}+\varepsilon_1(j)}{2}},$$

$$k_{2j} = k_0\sqrt{\frac{\sqrt{\varepsilon_1^2(j)+\varepsilon_2^2(j)}-\varepsilon_1(j)}{2}}.$$

Also $k_0 = 2\pi/\lambda$ is the vacuum wave number, and $L_{j,j+1}$ is the position of the center of a boundary between j and $j+1$ layers. Begining from the last of N layers, where $H_{\rm t}(j_{\rm N}) = 1$, $H_{\rm r}(j_{\rm N}) = 0$, we can iterate equations (13), (14) to obtain the incident and reflected waves in the medium 1.

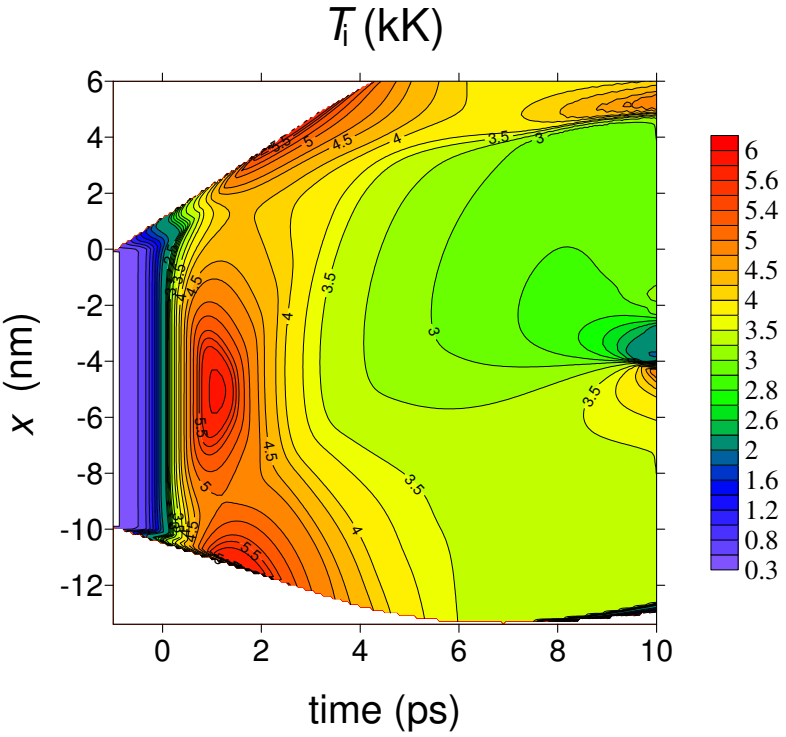

Figure 5. The temporal evolution of temperature distribution in the molybdenum film in the process of its ablation.

Dynamics of the molybdenum film on a glass being ablated under the action of femtosecond laser pulse provides us seven layers over a time interval of about 300 ps. According to the scheme of experiment the probe pulse is devided onto two components. One of them hits a target from its metal part, and the second one acts on the glass side. When considering the reflection of the probe pulse acting onto the metal film, the layers 1–8 are vacuum, detached part of film, vaporized cavity, crater film, cavity between crater film and glass, glass after shock, glass before shock, vacuum. In this case we are interesting in the temporal evolution of reflectivity

$$R(t) = \left| \frac{H_{\mathrm{r}}(1)}{H_{\mathrm{t}}(1)} \right|^2 .$$

For the second component of a probe pulse hitting a glass we shall consider its transmission through the arising multilayer structure 1–8 with layers in this case being vacuum, glass before shock, glass after shock, cavity between glass and crater film, crater film, vaporized cavity, detached part of film, vacuum. Transmission in dependence on time is

$$D(t) = \left| \frac{1}{H_{\mathrm{t}}(1)} \right|^2 \sqrt{\frac{\varepsilon_1}{\varepsilon_7}}.$$

Application of Lagrangian hydrodynamic code together with thermodynamic and kinetic characteristics of the film material makes it possible to obtain the parameters of the state at various points of the film during its motion. Temporal evolution of the ion temperature and its distribution in thin molybdenum film after the action of femtosecond laser pulse of $t_0 = 402.4$ fs duration with the value of the absorbed fluence 26.4 mJ/cm^2 is presented in figure 5. Duration t_0 corresponds to the Gaussian in time profile of impulse intensity, proportional to $\exp(-(t/t_0)^2)$.

In the time interval shown, the electron and ion temperatures are practically equalized. Because of thin film under consideration we can assume that the heating of the film is uniform

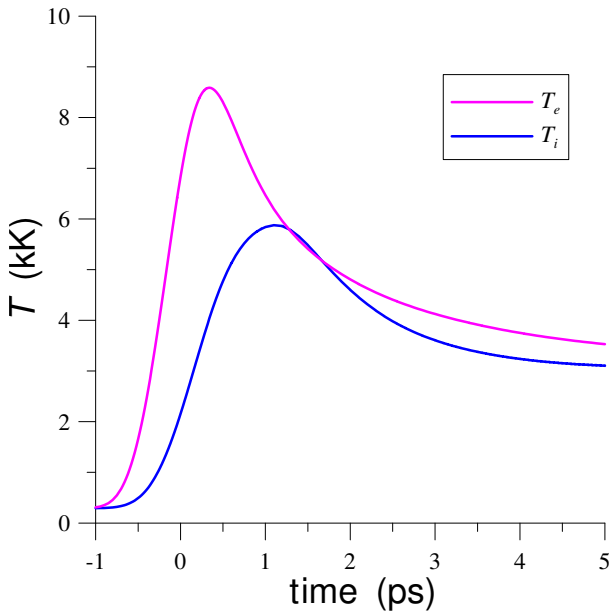

Figure 6. Electron and ion temperatures in the center of molybdenum film at an early stage of its ablation.

in its thickness. The process of equalizing the electron and ion temperatures in the central part of the film is shown in figure 6.

Cooling of the ionic system is associated with the expansion of the film. Since the ion pressure is greater, the cooling of the ion subsystem during expansion is more noticeable, and the cooling of the electronic subsystem is mainly determined by heat exchange with the ionic subsystem.

The density profile and its temporal evolution with a clearly visible detached part of the target is shown in figure 7.

Free surface of the film is initially at $x = 0$ and the boundary between the film and glass is at $x = -10$ nm. Because of the difference in these two boundaries of the film, the asymmetry of their behavior with time arises leading to the relatively small thickness of the detached layer of film. We have taken the next parameters of the target material. According to our hydrodynamical calculations the detached part of the film is about 2.4 nm and moves at the velocity $u_{\rm f} = 1.0$ km/s at the pump laser irradiation fluence 26.4 mJ/cm^2 under consideration. To calculate evolution of reflectivity and arising pattern of Newton rings in connection with experiments complex refractive index of this part of molybdennum film was taken $2.4 + 0.1$i, while for the vaporized cavity between the spalled part and the rest of the film is simply equal to 1. When the rest part of the film adjacent to the glass, in turn tears of from the glass, it moves at a speed of 0.14 km/s. It can be represented as consisting of two different parts: one, adjacent to the vapour cavity, having the thickness 2 nm with the same refractive index $2.4+0.1$i and the other part, of the thickness 9.1 nm, having the refractive index of about $5.1 + 3.7$i. The shock wave propagates into the glass with the speed $u_{\rm s} = 5.8$ km/s. The cavity between the upper subfilm and the bottom subfilm has refractive index equal 1 as well as the cavity between the bottom subfilm and the glass.

Temporal evolution of the reflectivity and transmission at the center of the laser spot are shown in figures 8 and 9. Together with the experimentally measured change of reflectivity and transmission in time this makes it possible to monitor the optical constants of the film matter during the ablation process. Reflectivity and transmission when taking into account the shock wave in a glass is presented in figures 10 and 11. The essential difference between figures 8 and

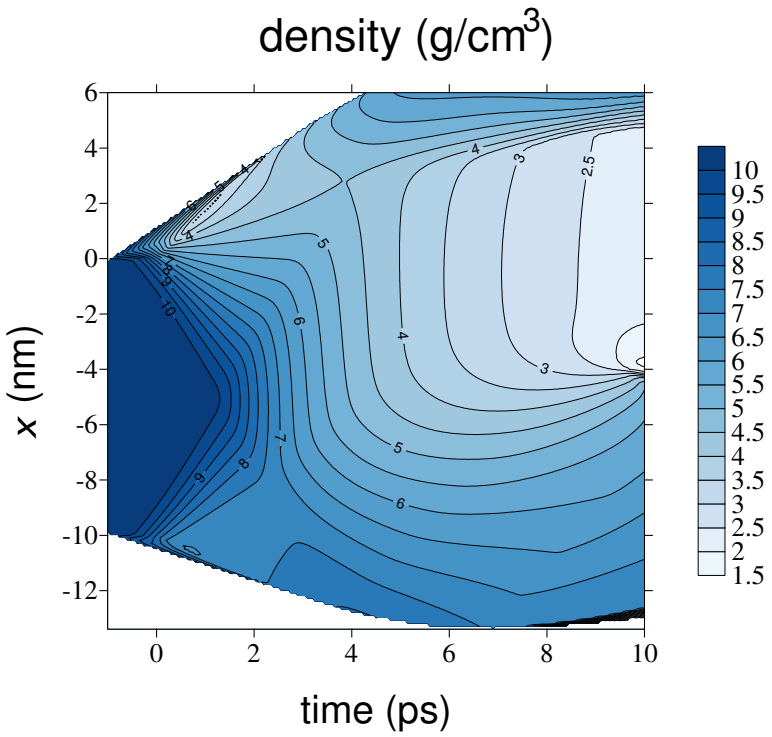

Figure 7. The density profile of the molybdenum target with the separated part.

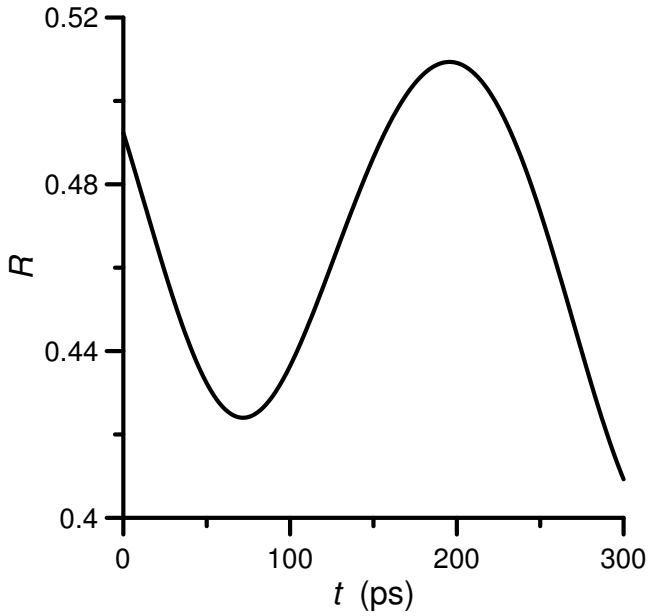

Figure 8. The temporal evolution of reflectivity at the ablation of thin molybdenum film exposed on the glass substrate. Probe laser pulse with the light wave 527 nm acts on the metal side of a target.

10 as well as between 9 and 11 shows the possibility of the shockwave monitoring during the pump–probe experiment.

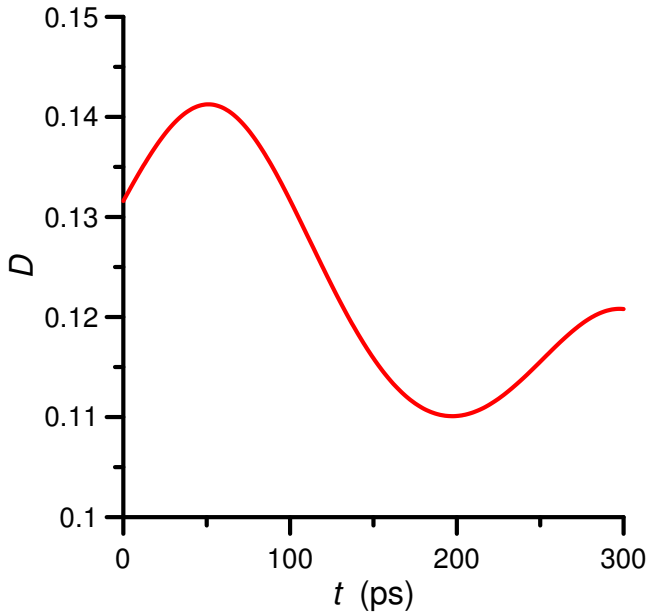

Figure 9. The dependence of transmission on time in the process of the ablation of molybdenum film on the glass. Probe laser pulse acts onto a target from its glass side.

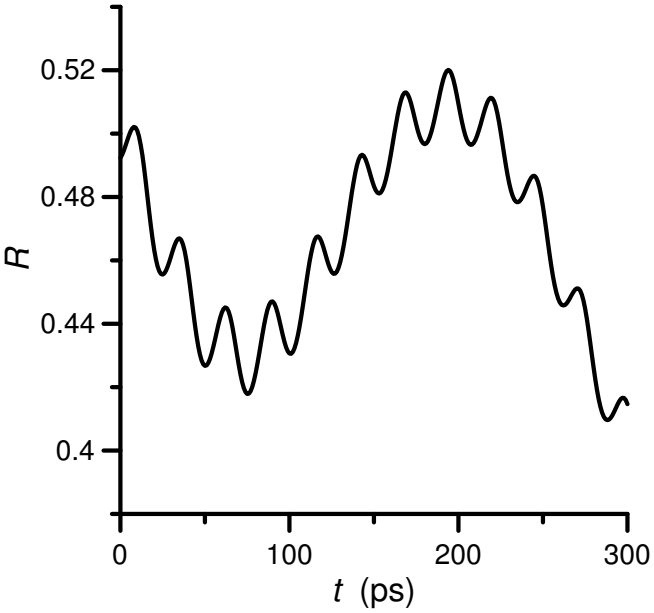

Figure 10. The evolution of reflectivity of probe laser pulse in time from the thin molybdenum film exposed on the glass substrate after the action of pump pulse. Shock wave propagating into the glass is taken into account. Probe laser pulse acts onto the metal side of a target.

4. Comparison with experiment

Experimental measurements of evolution of the Newton rings were made using technique described in paper [41]. Comparison of these measurements with simulated evolution is shown in figure 12. In experiment initial thickness of a Mo film was 10 nm, incident fluence was $F_{\text{inc}} = 77$ mJ/cm^2, duration of pulse was 0.4 ps.

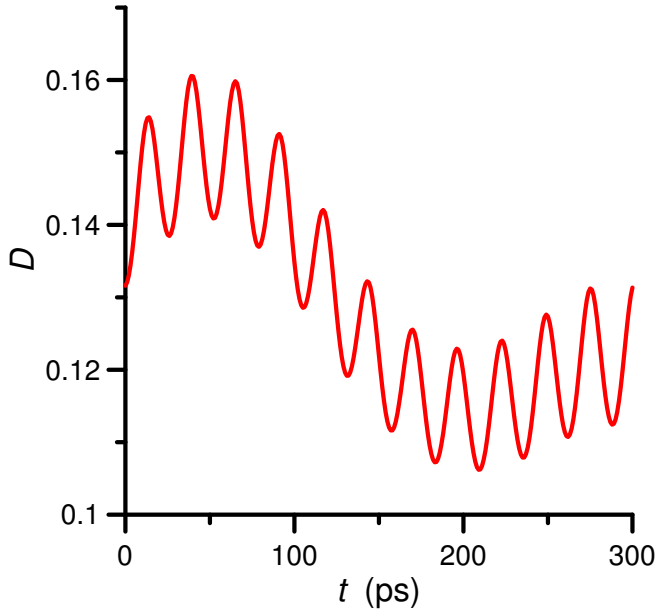

Figure 11. Transmission in dependence on time during the ablation of molybdenum film on the glass. Shock wave in a glass makes a contribution to the transmission. Probe laser pulse acts onto a glass side of a target.

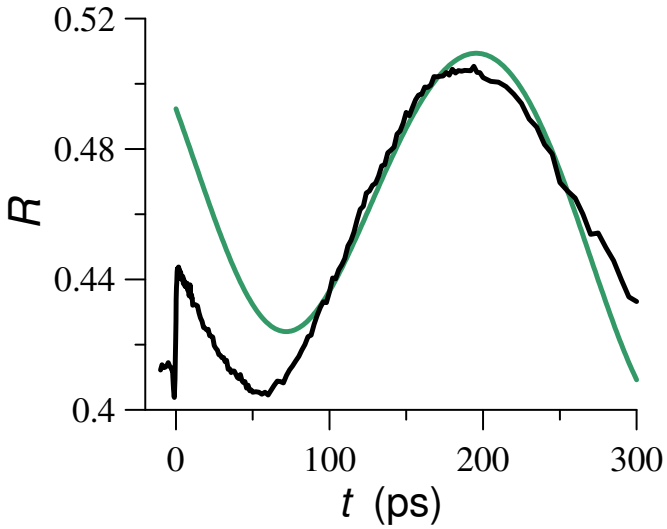

Figure 12. Comparison of calculations (green curve) and experiment (black curve), see text for explanations. The pulse is short, its duration is 0.4 ps. Its maximum is placed at the instant $t = 0$ at the time axis. The short parts before the instant $t = 0$ relates to the unperturbed situation. In this situation a reflective index R shown at the vertical axis is ≈ 0.4. Pulse is short, as was said, it sharply changes optical parameters of a film. The jump near the point $t = 0$ corresponds to transition to 2T state. 2T stage lasts few picoseconds, see figure 6. Additional efforts are necessary to adjust calculated 2T jump to the observation. We have to mention that the visibility of interference picture is rather low.

In calculation parameters were initial thickness of a Mo film was 10 nm, absorbed energy was $F_{\text{abs}} = 26.4$ mJ/cm^2, reflection coefficient for 10 nm Mo film placed above thick glass substrate is

0.413, reflection coefficient from a thick Mo film is 0.577. A film absorbs part of incident energy. Another part reflects back into vacuum and there is also a part which transits into glass. Pulse duration was the same as in experiment.

Simulation of the film ablation (figures 5 and 7) show that a film separates into two subfilms. The upper one in figure 7 is thinner than the subfilm contacting with the glass substrate below.Velocity of the upper subfilm approximately corresponds to experimental velocities. Both subfilms have reduced densities in comparison with the initial density of the film and are significantly heated. Therefore their optical parameters differ from those in normal conditions. Figure 12 shows that the using of optical constants given above, for the resulting multilayer structure, makes it possible to obtain satisfactory agreement between the experimental and theoretical results.

5. Conclusion

We have considered the behaviour of the thin molybdenum film on a glass substrate after the action of femtosecond laser pulse. The subjects of our study are two-temperature thermodynamic functions of molybdenum, dynamics of the ablation of the film and the optical response to the action of probe laser radiation. Presented model makes it possible to investigate all aspects of this problem.

Acknowledgments

The work concerning thermodynamics and kinetical properties of molybdenum is supported by grant No. 16-02-00864 from the Russian Foundation for Basic Research. The work on numerical simulation of heating and expansion of ultrathin molybdenum film is supported by Federal Agency for Scientific Organizations (FASO Russia), project No. 0033-2018-0004. The authors (JW, CA, SR, HPH) would like to thank the company Plansee SE in Austria for providing the Mo thin film samples. The authors also gratefully acknowledge the financial support by the Deutsche Forschungsgemeinschaft (DFG) (HU 1893/2-1). This work was also partly funded by the Erlangen Graduate School in Advanced Optical Technologies (SAOT) by the DFG in the framework of the German Excellence Initiative.

References

[1] Inogamov N A, Zhakhovskii V V, Ashitkov S I, Khokhlov V A, Petrov Yu V, Komarov P S, Agranat M B, Anisimov S I and Nishihara K 2009 *Appl. Surf. Sci.* **255** 9712–6

[2] Eidmann K, Meyer-ter-Vehn J, Schlegel T and Hüller S 2000 *Phys. Rev.* E **62** 1202–14

[3] Agranat M B, Andreev N E, Ashitkov S I, Veĭsman M E, Levashov P R, Ovchinnikov A V, Sitnikov D S, Fortov V E and Khishchenko K V 2007 *JETP Lett.* **85** 271–6

[4] Andreev N E and Kuznetsov S V 2003 *Plasma Phys. Control. Fusion* **45** A39

[5] Esirkepov T, Borghesi M, Bulanov S V, Mourou G and Tajima T 2004 *Phys. Rev. Lett.* **92** 175003

[6] Bychenkov V Yu, Brantov A V and Mourou G 2014 *Laser Part. Beams* **32** 605–11

[7] Sokolowski-Tinten K, Bialkowski J, Cavalleri A, von der Linde D, Oparin A, Meyer-ter-Vehn J and Anisimov S I 1998 *Phys. Rev. Lett.* **81** 224–7

[8] Inogamov N A, Petrov Yu V, Anisimov S I, Oparin A M, Shaposhnikov N V, von der Linde D and Meyer-ter-Vehn J 1999 *JETP Lett.* **69** 310–6

[9] Zhakhovskii V V, Nishihara K, Anisimov S I and Inogamov N A 2000 *JETP Lett.* **71** 167–72

[10] Zhigilei L V and Garrison B J 2000 *J. Appl. Phys.* **88** 1281–98 (*Preprint* https://doi.org/10.1063/1.373816)

[11] Anisimov S I, Kapeliovich B L and Perel'man T L 1974 *Sov. Phys. JETP* **39** 375–7

[12] Hohlfeld J, Wellershoff S S, Guedde J, Conrad U, Jaehnke V and Matthias E 2000 *Chem. Phys.* **251** 237–58

[13] Strickland D and Mourou G 1985 *Opt. Commun.* **56** 219–21

[14] Allen P B 1987 *Phys. Rev. Lett.* **59** 1460–3

[15] Wang X Y, Riffe D M, Lee Y S and Downer M C 1994 *Phys. Rev.* B **50** 8016–9

[16] Lugovskoy A V and Bray I 1999 *Phys. Rev.* B **60** 3279–88

[17] Rethfeld B, Kaiser A, Vicanek M and Simon G 2002 *Phys. Rev.* B **65** 214303

[18] Petrov Yu V 2005 *Laser Part. Beams* **23** 283–9

[19] Lin Z, Zhigilei L V and Celli V 2008 *Phys. Rev.* B **77** 075133
[20] Inogamov N A and Petrov Y V 2010 *J. Exp. Theor. Phys.* **110** 446–68
[21] Feynman R P, Metropolis N and Teller E 1949 *Phys. Rev.* **75** 1561
[22] Gilvarry J J 1954 *Phys. Rev.* **96** 934–43
[23] Gilvarry J J and Peebles G H 1955 *Phys. Rev.* **99** 550
[24] Al'tshuler L V, Kormer S B, Bakanova A A and Trunin R F 1960 *Sov. Phys. JETP* **11** 573
[25] Kormer S B, Funtikov A I, Urlin V D and Kolesnikova A N 1962 *Sov. Phys. JETP* **15** 477
[26] Al'tshuler L V, Bakanova A A and Trunin R F 1962 *Sov. Phys. JETP* **15** 65
[27] Fortov V E 2007 *Phys. Usp.* **50** 333
[28] Fortov V E and Lomonosov I V 2014 *Phys. Usp.* **57** 219
[29] Minakov D V and Levashov P R 2018 *J. Phys.: Conf. Ser.* **946** 012093
[30] Kanel' G I, Fortov V E and Razorenov S V 2007 *Phys. Usp.* **50** 771
[31] Inogamov N A, Petrov Yu V, Zhakhovsky V V, Khokhlov V A, Demaske B J, Ashitkov S I, Khishchenko K V, Migdal K P, Agranat M B, Anisimov S I, Fortov V E and Oleynik I I 2012 *AIP Conf. Proc.* **1464** 593–608 (*Preprint* http://aip.scitation.org/doi/pdf/10.1063/1.4739912)
[32] Migdal K P, Il'nitsky D K, Petrov Yu V and Inogamov N A 2015 *J. Phys.: Conf. Ser.* **653** 012086
[33] Petrov Y V, Migdal K P, Inogamov N A and Zhakhovsky V V 2015 *Appl. Phys. B* **119** 401–11
[34] Ashitkov S I, Komarov P S, Zhakhovsky V V, Petrov Y V, Khokhlov V A, Yurkevich A A, Ilnitsky D K, Inogamov N A and Agranat M B 2016 *J. Phys.: Conf. Ser.* **774** 012097
[35] Tanaka Y and Tsuneyuki S 2018 *Appl. Phys. Express* **11** 046701
[36] Ilnitsky D K, Khokhlov V A, Zhakhovsky V V, Petrov Yu V, Migdal K P and Inogamov N A 2016 *J. Phys.: Conf. Ser.* **774** 012101
[37] Petrov Yu V, Inogamov N A, Anisimov S I, Migdal K P and Khishchenko K V 2015 *J. Phys.: Conf. Ser.* **653** 012087
[38] Duffy T S, Shen G, Shu J, Mao H K, Hemley R J and Singh A K 1999 *J. Appl. Phys.* **86** 6729
[39] Huang X, Li F, Zhou Q, Meng Y, Litasov K D, Wang X, Liu B and Cui T 2016 *Sci. Rep.* **6** 19923
[40] Fat'yanov O V and Asimow P D 2017 *J. Appl. Phys.* **121** 115904
[41] Domke M, Felsl D, Rapp S, Sotrop J, Huber H P and Schmidt M 2015 *J. Laser Micro/Nanoeng.* **10** 119–22